Journal of Computational Physics **159,** 197–212 (2000)
doi:10.1006/jcph.2000.6428, available online at http://www.idealibrary.com on IDEAL®

A Discretization Scheme for an Extended Drift-Diffusion Model Including Trap-Assisted Phenomena

F. Bosisio, S. Micheletti, and R. Sacco

Dipartimento di Matematica, "F. Brioschi," Politecnico di Milano, Via Bonardi 9, 20133 Milano, Italy
E-mail: ricsac@mate.polimi.it

Received July 6, 1998; revised August 3, 1999

An extended drift-diffusion model is considered to account for the kinetics of electrons trapped in defect states within a semiconductor material. A discretization scheme based on Newton–Krylov iterations and mixed finite volumes is then proposed and applied to the model, even in the presence of Schottky contacts (i.e., Robin-type boundary conditions). Numerical results concerning the simulation of an electro-optical device in several working conditions are presented last. © 2000 Academic Press

Key Words: semiconductors; mixed finite elements; Newton–Krylov methods.

1. INTRODUCTION

This article deals with the numerical simulation of the dynamics of a CdTe resistor subject to a very high bias. Such a device is employed as a fast switch in state-of-the-art optical communication systems [34, 24, 21].

The mathematical model consists of the classical drift-diffusion equations [15, 31, 12] (henceforth denoted by DD) plus a set of ordinary differential equations (ODEs) describing the kinetics of the carriers trapped in defect states that are present within the semiconductor energy gap (henceforth referred to as *traps*) [10]. The spatial integration domain is assumed to be one-dimensional, L being the device length. This is due to the nature of the physical problem at hand, although the methodologies that we are going to introduce are by no means restricted to one-dimensional geometries. Suitable initial and boundary conditions (of Dirichlet and Robin type) must be provided for the unknowns of the problem, namely electric potential ψ, free electron and hole concentrations n and p, and trap concentrations n_{T_i} $(i = 1, \ldots, \mathbf{n}_{\mathrm{D}})$ and p_{T_j} $(j = 1, \ldots, \mathbf{n}_{\mathrm{A}})$, where $\mathbf{n}_{\mathrm{D}}$ and $\mathbf{n}_{\mathrm{A}}$ denote the number of donor-type and acceptor-type trapping states, respectively.

Despite its apparent simplicity, the CdTe resistor simulation is a heavily stiff problem, mainly due to the fact that this kind of device is quite "long" in real-life applications. This

0021-9991/00 $35.00

is a source of troubles when iterative decoupling algorithms are employed to solve the differential system, since the convergence rate is dramatically reduced as L gets large [13]. Such a drawback clearly demands the use of coupled approaches like Newton's method, which is (asymptotically) quadratically convergent, but requires a big computational effort. Moreover, stable and robust discretization schemes are mandatory for coping with the internal and boundary layers that arise when solving the current continuity equations.

In this article we propose an efficient implementation of the Newton method on the whole coupled system that is based on the use of a block Gauss–Seidel algorithm to decouple the traps from the free carriers. For each Gauss–Seidel step, we first solve by Krylov subspace iterations [14, 25] the free carrier block equations; then we solve the kinetic ODEs to update the trap concentrations. This second step is virtually cost-free since it requires the solution of $\mathbf{n}_{\mathrm{D}} + \mathbf{n}_{\mathrm{A}}$ diagonal linear systems. As for the spatial discretization, mixed finite volumes (MFV) are employed which ensure current flux conservation and nonnegative concentrations of free carriers [28]. Time advancing is dealt with the Backward Euler method (BE), which is well-known to be unconditionally stable. It is worth noting that the use of MFV and BE guarantees the positivity of the computed trapped carriers as well.

The outline of the article is as follows. The mathematical model of the problem at hand is presented in Section 2. An efficient implementation of a suitable iterative decoupling algorithm is then addressed in Section 3, where the Schur complement for Newton's method and the Kerkhoven–Saad approaches [14] are analyzed and compared. The spatial discretization scheme of the current continuity equations is described in Section 4, where a difference scheme is derived from the mixed finite element formulation of the problem by coupling the use of a quadrature formula to diagonalize the local stress matrix [3] with a harmonic average of the diffusion coefficient [20]. This technique is equivalent in one dimension to using the well-known exponentially fitted Scharfetter–Gummel method [30] and can be extended to the multidimensional case (see [20, 27–29, 19]). Numerical results are then reported in Section 5 to validate the computational procedure in the simulation of a realistic device operating in distinct (and quite different) working conditions.

2. THE SEMICONDUCTOR EQUATIONS COMPRISING TRAPS

The drift-diffusion equations including trap-assisted phenomena read (see, e.g., [31])

$$
\begin{cases}
\dfrac{\partial n_{\mathrm{T}_i}}{\partial t} = U^{\mathrm{D}}_{n_i} - U^{\mathrm{D}}_{p_i} \qquad i = 1, \ldots, \mathbf{n}_{\mathrm{D}} & \text{(1a)}\\
\dfrac{\partial p_{\mathrm{T}_j}}{\partial t} = U^{\mathrm{A}}_{p_j} - U^{\mathrm{A}}_{n_j} \qquad j = 1, \ldots, \mathbf{n}_{\mathrm{A}} & \text{(1b)}\\
-\operatorname{div}(\varepsilon \nabla \psi) = q \left[\sum_{1}^{\mathbf{n}_{\mathrm{D}}} {}_i \big(N_{\mathrm{D}_i} - n_{\mathrm{T}_i}\big) - \sum_{1}^{\mathbf{n}_{\mathrm{A}}} {}_j \big(N_{\mathrm{A}_j} - p_{\mathrm{T}_j}\big) + p - n \right] & \text{(1c)}\\
\dfrac{\partial n}{\partial t} - \dfrac{1}{q} \operatorname{div} \underline{J}_n = - \sum_{1}^{\mathbf{n}_{\mathrm{D}}} {}_i U^{\mathrm{D}}_{n_i} - \sum_{1}^{\mathbf{n}_{\mathrm{A}}} {}_j U^{\mathrm{A}}_{n_j} - U & \text{(1d)}\\
\dfrac{\partial p}{\partial t} + \dfrac{1}{q} \operatorname{div} \underline{J}_p = - \sum_{1}^{\mathbf{n}_{\mathrm{A}}} {}_j U^{\mathrm{A}}_{p_j} - \sum_{1}^{\mathbf{n}_{\mathrm{D}}} {}_i U^{\mathrm{D}}_{p_i} - U, & \text{(1e)}
\end{cases}
$$

with the constitutive relations,

$$\begin{cases} \underline{J}_n = qD_n\nabla n - q\mu_n n\nabla\psi \\ \underline{J}_p = -qD_p\nabla p - q\mu_p p\nabla\psi, \end{cases} \tag{2}$$

and the following expressions of the charge-trapping net recombination rates:

$$\begin{cases} U^{\mathrm{D}}_{n_i} = C^{\mathrm{D}}_{n_i}\left[\left(N_{\mathrm{D}_i} - n_{\mathrm{T}_i}\right)n - N_{\mathrm{C}}\exp\left(-\frac{E_{\mathrm{C}} - \mathcal{E}^{\mathrm{D}}_{\mathrm{T}_i}}{K_{\mathrm{B}}T}\right)n_{\mathrm{T}_i}\right] \\ U^{\mathrm{D}}_{p_i} = C^{\mathrm{D}}_{p_i}\left[n_{\mathrm{T}_i}p - N_{\mathrm{V}}\exp\left(-\frac{\mathcal{E}^{\mathrm{D}}_{\mathrm{T}_i} - E_{\mathrm{V}}}{K_{\mathrm{B}}T}\right)\left(N_{\mathrm{D}_i} - n_{\mathrm{T}_i}\right)\right] \qquad i = 1, \ldots, \mathbf{n}_{\mathrm{D}} \\ U^{\mathrm{A}}_{p_j} = C^{\mathrm{A}}_{p_j}\left[\left(N_{\mathrm{A}_j} - p_{\mathrm{T}_j}\right)p - N_{\mathrm{V}}\exp\left(-\frac{\mathcal{E}^{\mathrm{A}}_{\mathrm{T}_j} - E_{\mathrm{V}}}{K_{\mathrm{B}}T}\right)p_{\mathrm{T}_j}\right] \\ U^{\mathrm{A}}_{n_j} = C^{\mathrm{A}}_{n_j}\left[p_{\mathrm{T}_j}n - N_{\mathrm{C}}\exp\left(-\frac{E_{\mathrm{C}} - \mathcal{E}^{\mathrm{A}}_{\mathrm{T}_j}}{K_{\mathrm{B}}T}\right)\left(N_{\mathrm{A}_j} - p_{\mathrm{T}_j}\right)\right] \qquad j = 1, \ldots, \mathbf{n}_{\mathrm{A}}. \end{cases} \tag{3}$$

Suitable initial and boundary conditions must of course be provided. In (1), the unknowns ψ, n, p, n_{T_i}, and p_{T_j} are the electric potential and the electron and hole free and trapped carrier concentrations. The constants q and ε are the electronic charge and the material dielectric permettivity, respectively. The functions μ_n and μ_p are the carrier mobilities, related to the diffusivities D_n and D_p, respectively, through Einstein's relation.

Trapping recombination/generation phenomena are modeled by (3), where K_{B}, T, E_{C}, and E_{V} are the Boltzmann constant, the electronic temperature (assumed isothermal with the crystal lattice), and the conduction and valence band energy levels, respectively. The constants N_{C} and N_{V} are the effective densities of states. We assume that all of the traps have only one energy level, and there is no interaction among traps; moreover, we shall assume that the readjustment time for a trapped electron is negligible compared to time required on the average for the trap to emit the electron or to capture a hole (see [26]).

Semiconductor nondegeneracy is assumed henceforth (i.e., $n,\ p \ll N_{\mathrm{C}},\ N_{\mathrm{V}}$), which allows us to approximate the Fermi–Dirac statistics for the free-carriers with the Maxwell–Boltzmann statistics. The number of donor levels occupied by the trapped electrons, instead, is given by Fermi–Dirac statistics

$$n_{\mathrm{T}} = \frac{N_{\mathrm{D}}}{1 + \exp\left(\frac{\mathcal{E}^{\mathrm{D}}_{\mathrm{T}} - \mathcal{E}_{\mathcal{F}}}{K_{\mathrm{B}}T}\right)}, \tag{4}$$

because the energy distance between the trapping level $\mathcal{E}^{\mathrm{D}}_{\mathrm{T}}$ and the fermi level $\mathcal{E}_{\mathcal{F}}$ can be small, thus making the effects of Pauli principle nonnegligible. An analogous relation to (4) holds for the trapped holes occupying the acceptor levels: Mathematically, (4) implies that $N_{\mathrm{D}} - n_{\mathrm{T}} \geq 0$ ($N_{\mathrm{A}} - p_{\mathrm{T}} \geq 0$) for all x and t.

The coefficients $C^{\mathrm{D}}_{n_i}$, $C^{\mathrm{D}}_{p_i}$ ($C^{\mathrm{A}}_{n_j}$, $C^{\mathrm{A}}_{p_j}$, resp.) and the parameters $\mathcal{E}^{\mathrm{D}}_{\mathrm{T}_i}$ ($\mathcal{E}^{\mathrm{A}}_{\mathrm{T}_j}$, resp.) denote the capture coefficients and the energy levels of each trap within the energy gap. Superscripts D and A characterize "donor-type" and "acceptor-type" trapping centers, respectively. N_{D_i} and N_{A_j} are respectively the concentrations of each donor-type and acceptor-type impurity throughout the semiconductor. (For a complete derivation of the drift-diffusion model, see

[15, 12, 31], and a detailed physical description of the recombination/generation processes can be found in [33] and [31], Chapter 4).

We point out that assuming the trapping center to be in stationary conditions, i.e., $\frac{\partial n_T}{\partial t} = \frac{\partial p_T}{\partial t} = 0$, we recover the classical Shockley–Read–Hall model for trap-assisted generation–recombination phenomena. The function U in (1d)–(1e) denotes the net recombination rate due to processes different from the trap-assisted phenomena (Shockley–Read–Hall processes). It includes three-particle phenomena (Auger recombination, impact ionization), and the *direct* processes assisted by photons (*band-to-band* optical recombination and generation) [31]. Henceforth, we will neglect such phenomena, except for the optical generation, thus assuming $U = -G^{\text{opt}}$.

3. THE ITERATIVE SCHEME AND THE NEWTON METHOD

System (1) constitutes a set of nonlinearly coupled equations so that a suitable decoupling algorithm is highly recommended for its solution.

A first approach could be the use of a *generalized Gummel map* [11], which amounts to solving each equation assuming only the corresponding variable to be unknown and then iterating until convergence is achieved. Despite its simplicity, this approach is not very satisfactory because of the very high number of iterations required for convergence, especially under high bias and high photogeneration conditions [17]. A second possibility consists of using a global Newton algorithm. This is general will certainly improve convergence speed at the expense of an increase in the computational cost.

We thus follow an intermediate strategy, which has proved to work quite effectively in numerical experiments; i.e., we decouple the traps from the other equations of the system by means of a block Gauss–Seidel algorithm and apply Newton's method only to Poisson and currents equations. This considerably simplifies the iterative scheme, since the Jacobian matrix can be handled in a block fashion, reducing both the computational time and the required memory. Moreover, our implementation of Newton's method ensures that the right-hand sides in both current equations are positive, so that a *discrete maximum principle* for the concentrations holds provided that a suitable discretization scheme is employed.

In the forthcoming sections we address two different implementations of Newton's method on the DD equations only (i.e., Poisson and current continuity equations), assuming the traps to be known. This amounts to analyzing the single step of the outer Gauss–Seidel loop, corresponding to the time discretization of system (1) by the BE method.

3.1. *The Schur Complement Approach*

Assuming the traps to be known, the DD system can be symbolically written through three nonlinear operators as:

$$\begin{cases} \mathbf{V}(\psi, n, p) = 0 & \text{(5a)} \\ \mathbf{W}(n, \psi) = 0 & \text{(5b)} \\ \mathbf{Z}(p, \psi) = 0. & \text{(5c)} \end{cases}$$

Denoting by (v, w, z) the variations of (ψ, n, p) and neglecting the (possible) dependencies of the mobilities μ_n and μ_p on (ψ, n, p), a step of Newton's method for the DD system can

be written in matrix form as

$$\begin{bmatrix} \mathbf{A}_{11} & \mathbf{A}_{12} & \mathbf{A}_{13} \\ \mathbf{A}_{21} & \mathbf{A}_{22} & \mathbf{0} \\ \mathbf{A}_{31} & \mathbf{0} & \mathbf{A}_{33} \end{bmatrix} \begin{bmatrix} v \\ w \\ z \end{bmatrix} = \begin{bmatrix} -\mathbf{V}(\psi, n, p) \\ -\mathbf{W}(n, \psi) \\ -\mathbf{Z}(p, \psi) \end{bmatrix}, \tag{6}$$

where the matrix blocks $\mathbf{A}_{ij}$ are given by, for $i, j = 1, 2, 3$,

$$\begin{aligned} \mathbf{A}_{11} v &= \frac{\partial \mathbf{V}}{\partial \psi}(v) = -\operatorname{div}(\varepsilon \nabla v) \\ \mathbf{A}_{12} w &= \frac{\partial \mathbf{V}}{\partial n}(w) = w & \mathbf{A}_{13} z &= \frac{\partial \mathbf{V}}{\partial p}(z) = -z \\ \mathbf{A}_{21} v &= \frac{\partial \mathbf{W}}{\partial \psi}(v) = \operatorname{div}(q \mu_n n \nabla v) & \mathbf{A}_{22} w &= \frac{\partial \mathbf{W}}{\partial n}(w) = -\operatorname{div} \underline{J}_n(w) \\ \mathbf{A}_{31} v &= \frac{\partial Z}{\partial \psi}(v) = -\operatorname{div}(q \mu_p p \nabla v) & \mathbf{A}_{33} z &= \frac{\partial \mathbf{Z}}{\partial p}(z) = \operatorname{div} \underline{J}_p(z). \end{aligned} \tag{7}$$

The presence of the two zero blocks allows us to eliminate w and z from the last two equations as a function of v:

$$\begin{cases} w = -\mathbf{A}_{22}^{-1}(\mathbf{W} + \mathbf{A}_{21} v) \\ z = -\mathbf{A}_{33}^{-1}(\mathbf{Z} + \mathbf{A}_{31} v). \end{cases} \tag{8}$$

Plugging (8) back into the first equation of (6) we finally obtain

$$\left(\mathbf{A}_{11} - \mathbf{A}_{12}\mathbf{A}_{22}^{-1}\mathbf{A}_{21} - \mathbf{A}_{13}\mathbf{A}_{33}^{-1}\mathbf{A}_{31}\right) v = -\mathbf{V} + \mathbf{A}_{12}\mathbf{A}_{22}^{-1}\mathbf{W} + \mathbf{A}_{13}\mathbf{A}_{33}^{-1}\mathbf{Z}, \tag{9}$$

where the so called *Schur complement* matrix $\mathbf{S}$ can be recognized on the left-hand side:

$$\mathbf{S} = \mathbf{A}_{11} - \mathbf{A}_{12}\mathbf{A}_{22}^{-1}\mathbf{A}_{21} - \mathbf{A}_{13}\mathbf{A}_{33}^{-1}\mathbf{A}_{31}. \tag{10}$$

Matrix $\mathbf{S}$ is in general full, due to the inversion of blocks $\mathbf{A}_{22}$ and $\mathbf{A}_{33}$, although each single block $\mathbf{A}_{ij}$ has a sparse structure. This makes it in practice impossible to build and store the Schur matrix $\mathbf{S}$ and thus requires the use of an *iterative* method such as GMRES to solve system (9) [25]. This method requires only the multiplication of the matrix $\mathbf{S}$ with some vector $\mathbf{x}$, which can be done as follows:

$$\mathbf{S}\mathbf{x} = \mathbf{A}_{11}\mathbf{x} - \mathbf{A}_{12}\mathbf{y} - \mathbf{A}_{13}\mathbf{z}, \tag{11}$$

where $\mathbf{y}$ and $\mathbf{z}$ can be found by solving the systems $\mathbf{A}_{22}\mathbf{y} = \mathbf{A}_{21}\mathbf{x}$ and $\mathbf{A}_{33}\mathbf{z} = \mathbf{A}_{31}\mathbf{x}$.

3.2. *An Abstract Framework*

Each of the equations (5) implicitly defines a nonlinear operator:

$$\begin{cases} \psi = \mathbf{\Psi}(n, p) \\ n = \mathbf{N}(\psi) \\ p = \mathbf{P}(\psi). \end{cases} \tag{12}$$

Plugging the operators related to the concentrations back into the potential equation we get

$$\psi = \mathbf{\Psi}(\mathbf{N}(\psi), \mathbf{P}(\psi)). \tag{13}$$

Setting $\mathbf{T}(\psi) = \Psi(\mathbf{N}(\psi), \mathbf{P}(\psi))$, the solution of the DD system thus amounts to dealing with the nonlinear operator equation:

$$\psi = \mathbf{T}(\psi). \tag{14}$$

A first approach to solving (14) consists of resorting to a fixed point iteration:

$$\psi_{k+1} = \mathbf{T}(\psi_k). \tag{15}$$

This latter is exactly the classical *Gummel map* (where the equations are solved in reverse order with respect to the standard decoupling algorithm).

An alternative strategy (originally proposed by Kerkhoven and Saad [14]) consists of reformulating (14) as:

$$(\mathbf{I} - \mathbf{T})(\psi) = \mathbf{0}, \tag{16}$$

$\mathbf{I}$ being the identity operator. It is now clearly possible to apply Newton's method to (16) to obtain

$$\begin{cases} \mathbf{J}(v) &= -(\mathbf{I} - \mathbf{T})(\psi_k) \\ \psi_{k+1} = \psi_k + v, \end{cases} \tag{17}$$

where $\mathbf{J}$ denotes the Fréchet derivative of the operator $\mathbf{I} - \mathbf{T}$:

$$\mathbf{J} = \frac{\partial}{\partial \psi}[\mathbf{I} - \mathbf{T}] = \frac{\partial}{\partial \psi}[\mathbf{I} - \mathbf{\Psi}(\mathbf{N}(\psi), \mathbf{P}(\psi))] = \mathbf{I} - \frac{\partial \mathbf{\Psi}}{\partial n}\frac{\partial \mathbf{N}}{\partial \psi} - \frac{\partial \mathbf{\Psi}}{\partial p}\frac{\partial \mathbf{P}}{\partial \psi}. \tag{18}$$

Differentiating the current equations in (5) with respect to ψ, and the potential equation with respect to n and p yields

$$\mathbf{J} = \left(\frac{\partial \mathbf{V}}{\partial \psi}\right)^{-1}\left[\frac{\partial \mathbf{V}}{\partial \psi} - \frac{\partial \mathbf{V}}{\partial n}\left(\frac{\partial \mathbf{W}}{\partial n}\right)^{-1}\frac{\partial \mathbf{W}}{\partial \psi} - \frac{\partial \mathbf{V}}{\partial p}\left(\frac{\partial \mathbf{Z}}{\partial p}\right)^{-1}\frac{\partial \mathbf{Z}}{\partial \psi}\right], \tag{19}$$

from which we conclude that method (17) leads to solve the linear system

$$\left\{\mathbf{I} - \left(\frac{\partial \mathbf{V}}{\partial \psi}\right)^{-1}\left[\frac{\partial \mathbf{V}}{\partial n}\left(\frac{\partial \mathbf{W}}{\partial n}\right)^{-1}\frac{\partial \mathbf{W}}{\partial \psi} + \frac{\partial \mathbf{V}}{\partial p}\left(\frac{\partial \mathbf{Z}}{\partial p}\right)^{-1}\frac{\partial \mathbf{Z}}{\partial \psi}\right]\right\} v = -\mathbf{V}(\psi, \mathbf{N}(\psi), \mathbf{P}(\psi)). \tag{20}$$

Using definitions (7), we can write (20) in matrix form as

$$\mathbf{A}_{11}^{-1}\left(\mathbf{A}_{11} - \mathbf{A}_{12}\mathbf{A}_{22}^{-1}\mathbf{A}_{21} - \mathbf{A}_{13}\mathbf{A}_{33}^{-1}\mathbf{A}_{31}\right) v = -\mathbf{V}; \tag{21}$$

that is,

$$\left(\mathbf{A}_{11} - \mathbf{A}_{12}\mathbf{A}_{22}^{-1}\mathbf{A}_{21} - \mathbf{A}_{13}\mathbf{A}_{33}^{-1}\mathbf{A}_{31}\right) v = -\mathbf{A}_{11}\mathbf{V}. \tag{22}$$

It is easily seen that this linearization process shares the *same* coefficient matrix as the Newton method (9) when implemented with a Schur complement approach, but has a

different right-hand side. Computing this latter amounts to solving at each time step the two continuity equations (1d)–(1e) with a given potential.

With this aim, we consider a suitable splitting of the recombination/generation terms that ensures the positiveness of the right-hand sides of the corresponding finite element systems and thus, in turn, the positiveness of the concentrations (*discrete maximum principle*). This statement will be addressed more in detail in the next section and represents the main difference between approaches (22) and (9).

Furthermore, we notice that the block $\mathbf{A}_{11}$ arises as a natural preconditioner for the Schur matrix. In such a case, the eigenvalues of the final matrix at the left-hand side of (21) are clustered around the value 1 in the complex plane due to the inversion of blocks $\mathbf{A}_{22}$ and $\mathbf{A}_{33}$ coming from the discretization of two elliptic problems [14].

4. NUMERICAL SOLUTION OF THE CURRENT CONTINUITY EQUATIONS

In this section we deal with the numerical approximation of the current continuity equations in a one dimensional domain $[0, L]$ using mixed finite elements. The multidimensional extension of the method has been considered and analyzed in [20, 27–29, 19].

Using the classical Slotboom change of variable [32], the current densities can be written as

$$J = \pm q D_\nu n_{\text{intr}} e^{\pm\psi/V_{\text{th}}} u', \tag{23}$$

where the prime denotes spatial differentiation, ν stands for n or p, V_{th} is the thermal voltage, n_{intr} is the intrinsic concentration in the semiconductor and $u = \frac{\nu}{n_{\text{intr}}} e^{\mp\psi/V_{\text{th}}}$ is the Slotboom variable associated with electrons (top sign) or holes (bottom sign), here and throughout.

Owing to (23) the boundary value problem associated with each linearized current continuity equation can be formulated as

$$\begin{cases} J = \pm a u' & \text{in } (0, L) \\ \mp J' + \sigma u = f & \text{in } (0, L) \\ u(0) = g, \qquad J(L) = \mp\alpha(u(L) - u_{\text{S}}), & \end{cases} \tag{24}$$

where

$$a = q D_\nu n_{\text{intr}} e^{\pm\psi/V_{\text{th}}}, \tag{25}$$

while g, α, and u_{S} are positive given constants and a, σ, and f are positive given functions with a^{-1}, $\sigma \in L^\infty(0, L)$ and $f \in L^2(0, L)$ (for the definition of all the function spaces, see, e.g., [22], Chapter 1, and [6], Chapter 3).

To prove the positiveness of σ and f, consider the current continuity equation for electrons and assume for the sake of simplicity (but without loss of generality) that $\mathbf{n}_{\text{D}} = \mathbf{n}_{\text{A}} = 1$ in (1). Then, using the BE method for the time discretization and moving the recombination terms to the left-hand side, we get

$$\begin{aligned} &-\frac{1}{q} J' + \left(\frac{1}{\Delta t} + \mathcal{A}(N_{\text{D}} - n_{\text{T}}) + \mathcal{B} p_{\text{T}} \right) n_{\text{intr}} e^{\psi/V_{\text{th}}} u \\ &\quad = \frac{1}{\Delta t} n_{\text{intr}} e^{\psi/V_{\text{th}}} u^{\text{old}} + G^{\text{opt}} + \mathcal{C} n_{\text{T}} + \mathcal{D}(N_{\text{A}} - p_{\text{T}}), \end{aligned} \tag{26}$$

where u and u^{old} denote the unknown and its value at the previous time step, respectively, while the positive constants $\mathcal{A}$, $\mathcal{B}$, $\mathcal{C}$, and $\mathcal{D}$ account for the physical parameters of the recombination/generation processes. Equation (26) is clearly in the form (24), where σ coincides with the recombination terms plus the contribution coming from time discretization and f includes the generation terms plus time discretization, respectively. The positiveness of σ and f then immediately follows recalling (4). Similar conclusions can be drawn for the hole current equation.

Mixed Dirichlet–Robin boundary conditions are considered in (24), with a Dirichlet condition for u at the ohmic contact at $x = 0$ and a Robin-type condition at the Schottky contact at $x = L$. In this case $\alpha = q v_v n_{\text{intr}} e^{\pm \psi_S / V_{\text{th}}}$, where v_v is the thermoionic emission velocity of the contact and ψ_S is the Dirichlet value of ψ at the Schottky contact, while $u_S = (v_S / n_{\text{intr}}) e^{\mp \psi_S / V_{\text{th}}}$, v_S being the equilibrium concentration which is related to the barrier height between the metal and the semiconductor [31, 7].

4.1. *Dual Mixed Formulation and Raviart–Thomas Finite Element Discretization*

In this section we address the dual-mixed formulation of problem (24) and its discretization using Raviart–Thomas finite elements. Let

$$V = L^2(0,L), \qquad Q = H(\text{div}; (0,L)) = \{\tau \in L^2(0,L) : \tau' \in L^2(0,L)\}. \tag{27}$$

Then, the dual mixed formulation of (24) reads (see [6])

$$\begin{cases} \text{Find } u \in V \text{ and } J \in Q \text{ such that} & \\ \int_0^L a^{-1} J\tau \, dx \pm \int_0^L u\tau' \, dx + \alpha^{-1} J(L)\tau(L) = \mp g\tau(0) \pm u_S \tau(L) & \forall \tau \in Q \\ \int_0^L \mp J' v \, dx + \int_0^L \sigma u v \, dx = \int_0^L f v \, dx & \forall v \in V. \end{cases} \tag{28}$$

Problem (28) admits a unique solution (J, u) (see [6], Theorem 1.2, p. 47, [20]).

Let us now consider the Galerkin approximation of (28). With this aim, let $\mathcal{T}_h$ be a nonuniform partition of $[0, L]$ such that $x_0 = 0 < x_1 < \cdots < x_n = L$ and denote by $T_i = [x_{i-1}, x_i]$, $i = 1, \ldots, n$, an interval of the partition of width $h_i = x_i - x_{i-1}$. We also denote by C_i the midpoint of each element T_i and by d_i the distance between C_i and C_{i+1}, $i = 1, \ldots, n-1$, whereas we set $C_0 = x_0$, $d_0 = h_1/2$ and $C_{n+1} = x_n$, $d_n = h_n/2$.

For $k \geq 0$ we let $\mathbb{P}_k$ be the space of polynomials of degree $\leq k$ and introduce the Raviart–Thomas finite element space of lowest order [23]:

$$V_h = \left\{ v_h \in V : v_h|_{T_i} \in \mathbb{P}_0, \forall T_i \in \mathcal{T}_h \right\}, \qquad Q_h = \left\{ \tau_h \in Q : \tau_h|_{T_i} \in \mathbb{P}_1, \forall T_i \in \mathcal{T}_h \right\}. \tag{29}$$

The degrees of freedom for the unknowns u_h and J_h are the values u_i of u_h over each element T_i, and the values Φ_l of J_h at each node x_l of $\mathcal{T}_h$, respectively.

The finite element discretization of (28) reads

$$\begin{cases} \text{Find } u_h \in V_h \text{ and } J_h \in Q_h \text{ such that} & \\ \int_0^L a^{-1} J_h \tau_h \, dx \pm \int_0^L u_h \tau_h' \, dx + \alpha^{-1} J_h(L)\tau_h(L) = \mp g\tau_h(0) \pm u_S \tau_h(L) & \forall \tau_h \in Q_h \\ \int_0^L \mp J_h' v_h \, dx + \int_0^L \sigma u_h v_h \, dx = \int_0^L f v_h \, dx & \forall v_h \in V_h. \end{cases} \tag{30}$$

Again, existence and uniqueness of the solution (J_h, u_h) hold for problem (30) (see [6], Proposition 2.11, p. 61, [20]). The linear system resulting from (30) reads

$$\begin{cases} \sum_{\ell=0}^{n} \Phi_\ell \int_0^L a^{-1}\tau_\ell\tau_i \,\mathrm{d}x \pm \sum_{k=1}^{n} u_k \int_0^L \tau_i' \,\mathrm{d}x + \frac{1}{\alpha}\Phi_n\tau_i(L) \\ \quad = \mp g\tau_i(0) \pm u_S\tau_i(L) & i = 0,\dots,n \\ \pm(\Phi_{k-1} - \Phi_k) + u_k\sigma_k h_k = f_k h_k, & k = 1,\dots,n \end{cases} \tag{31}$$

where σ_k, f_k are the averages of σ and f on each $\mathcal{T}_k \in \mathcal{T}_h$.

4.2. *Diagonalization of the Mixed System: The Finite Volume Approach*

The discrete equations (31) are a coupled system in the unknowns Φ_l and u_i. Our approach is based on the coupled use of a suitable quadrature formula and of a special average of the coefficient a. The former allows us to diagonalize the system, thus eliminating the fluxes and yielding a system which acts only on the scalar unknown u_h. About the latter, let us first define for any continuous function $\phi(z)$: $[0, h] \mapsto \mathbb{R}^+$ such that $\phi(0) = \phi_0$ and $\phi(h) = \phi_h$, the *exponential interpolant*,

$$\Pi_e\phi(x) = \exp\{\Pi_1[\ln\phi(x)]\} = \phi_0\left(\frac{\phi_h}{\phi_0}\right)^{x/h}, \qquad 0 \le x \le h, \tag{32}$$

where $\Pi_1(\varphi)$ is the $\mathbb{P}_1$ interpolant of the function φ. This particular type of interpolation (which, actually, is a convex average of ϕ_0 and ϕ_h) is motivated by the special form of the coefficient a in the semiconductor equations. Indeed, if $a = e^\lambda$, $\lambda \in \mathbb{P}_1$ (as in the present case), then $\Pi_e(a^{-1}) = a^{-1}$. Using the average (32), with a as in (25), we thus recover the well-known Scharfetter–Gummel scheme [30].

For $i = 0,\dots,n-1$ we define $\langle a^{-1}\rangle_i$ as the mean value of $\Pi_e(a^{-1})$ between C_i and C_{i+1} and approximate the integral in the first equation of (31) as

$$\int_0^L a^{-1}\tau_\ell\tau_i \,\mathrm{d}x \simeq \langle a^{-1}\rangle_i d_i.$$

The generalized Galerkin dual mixed system then reads

$$\begin{cases} \Phi_i\langle a^{-1}\rangle_i d_i \pm (u_i - u_{i+1}) + \frac{1}{\alpha}\Phi_n\tau_i(L) = \mp g\tau_i(0) \pm u_S\tau_i(L) & i = 0,\dots,n \\ \pm(\Phi_{k-1} - \Phi_k) + u_k\sigma_k h_k = f_k h_k & k = 1,\dots,n \\ u_0 = u_{n+1} = 0 \end{cases} \tag{33}$$

and is, therefore, a genuine cell-centered finite volume formulation. Notice that the first equation in (33) makes sense also for $i = 0$ and $i = n$ upon introducing the artificial values u_0 and u_{n+1}.

A two-dimensional extension of the dual-mixed discretization procedure described so far has been carried out in [20] where an $\mathcal{O}(h)$ error estimate that generalizes the classical results of Falk and Osborn [8] has been established for the novel method. The scheme has also been used in the multidimensional case for the approximation of scalar advection–diffusion equations [27] and employed in [28, 5, 18, 19] for the simulation of silicon semiconductor devices using the drift-diffusion and the energy-balance transport models.

In the next sections we analyze the case where x_i is an internal node ($i = 1, \ldots, n$) and the cases $i = 0$ and $i = n$.

4.2.1. Internal nodes. In this case the equation for the nodal flux reads

$$\Phi_i \langle a^{-1} \rangle_i d_i \pm (u_i - u_{i+1}) = 0, \qquad i = 1, \ldots, n-1, \tag{34}$$

from which, denoting by $\mathcal{H}_i(a)$ the *harmonic average* $1/\langle a^{-1} \rangle_i$ of $\Pi_e(a)$, we obtain

$$\Phi_i = \pm \mathcal{H}_i(a) \frac{u_{i+1} - u_i}{d_i}, \qquad i = 1, \ldots, n-1. \tag{35}$$

4.2.2. Ohmic node (Dirichlet boundary condition). In this case the flux equation reads

$$\Phi_0 \langle a^{-1} \rangle_0 d_0 \mp u_1 = \mp g, \tag{36}$$

since the test function τ_0 has its support only on the interval T_1. From (36) the nodal flux reads

$$\Phi_0 = \pm \mathcal{H}_0(a) \frac{u_1 - g}{d_0}. \tag{37}$$

Notice that (37) differs from (35) only since u_i has been replaced by the boundary datum g and d_i has been replaced by d_0. In other words, the effect is the same as if a "mirroring" interval T_0 existed outside $[0, L]$, having its midpoint at $x = 0$, and the value of the associated unknown u_0 were set equal to g.

4.2.3. Schottky node (Robin boundary condition). In this case the flux equation is

$$\Phi_n \langle a^{-1} \rangle_n d_n \pm u_n + \frac{1}{\alpha} \Phi_n = \pm u_S, \tag{38}$$

since the test function τ_n has its support only on the interval T_n. The nodal flux is

$$\Phi_n = \pm \mathcal{H}_n(a) \frac{u_S - u_n}{d_n} \frac{1}{1 + \frac{\mathcal{H}_n(a)}{\alpha d_n}}, \tag{39}$$

which differs from (37) due to the presence of the third term at right-hand side. We shall comment on the meaning of (39) later on.

4.2.4. Properties of the discretization method. We can prove the following:

PROPOSITION 1 (Discrete maximum principle). *The discrete problem* (33) *has a unique and positive solution.*

Proof. Problem (33) can be written in matrix form as $\mathbf{Mu} = \mathbf{b}$ where $\mathbf{u} = (u_1, \ldots, u_n)^{\mathrm{T}}$ is the vector of the element unknowns, $\mathbf{b} = (b_1, \ldots, b_n)^{\mathrm{T}}$ is the right-hand side and $\mathbf{M}$ is the tridiagonal matrix of order n obtained after eliminating the fluxes from system (33). For $i = 2, \ldots, n-1$ the matrix entries are

$$M_{ij} = \begin{cases} -\frac{\mathcal{H}_{i-1}(a)}{d_{i-1}} & j = i-1 \\ \left(\frac{\mathcal{H}_{i-1}(a)}{d_{i-1}} + \frac{\mathcal{H}_i(a)}{d_i} + \sigma_i h_i \right) & j = i \\ -\frac{\mathcal{H}_i(a)}{d_i} & j = i+1, \end{cases}$$

while the entries of the first and last row are

$$M_{11} = \left(\frac{\mathcal{H}_0(a)}{d_0} + \frac{\mathcal{H}_1(a)}{d_1} + \sigma_1 h_1 \right), \qquad M_{12} = -\frac{\mathcal{H}_1(a)}{d_1}$$

$$M_{nn-1} = -\frac{\mathcal{H}_{n-1}(a)}{d_{n-1}}, \qquad M_{nn} = \left(\frac{\mathcal{H}_{n-1}(a)}{d_{n-1}} + \frac{\mathcal{H}_n(a)}{d_n} \frac{1}{1 + \frac{\mathcal{H}_n(a)}{\alpha d_n}} + \sigma_n h_n \right).$$

Matrix $\mathbf{M}$ is symmetric and strictly diagonally dominant with $M_{ii} > 0$ and $M_{ij} \leq 0$ for $i \neq j$, $i, j = 1, \ldots, n$. Thus, it is a Stiltjes matrix (see Corollary 3, p. 85 [35]) and admits a strictly positive inverse. Therefore, system (33) is uniquely solvable with a positive solution since $b_i > 0$, $i = 1, \ldots, n$, due to the fact that f, g, α, and u_S are positive.

4.3. *Formulation with the n and p Variables*

The dual mixed discretization considered so far is based on the symmetric formulation of the differential problem (24). In the case of the continuity equations this amounts to writing the current densities using the Slotboom variables, which, although attractive from the theoretical point of view, are not convenient in actual computations due to the presence of exponentially varying coefficients that may give rise to overflow problems (see (25)). It is therefore necessary to go back at the discrete level to the original (and physical) unknowns n and p. By doing so, the symmetry of the problem is lost but, nevertheless, the resulting matrices acting on n_h and p_h are still M-matrices, that is, nonsingular and with strictly positive inverse. This property, provided that the right-hand sides of the systems are positive, ensures a discrete maximum principle to hold, that is, $n_h > 0$, $p_h > 0$.

Recalling (25) and the definition of the harmonic average $\langle a^{-1} \rangle$, we get

$$\mathcal{H}_i(a) = \left[\frac{1}{d_i} \int_{C_i}^{C_{i+1}} \frac{1}{q D_\nu n_{\text{intr}}} e^{\mp \psi(x)/V_{\text{th}}} \, \mathrm{d}x \right]^{-1} = q D_\nu n_{\text{intr}} e^{\pm \psi_i / V_{\text{th}}} \mathcal{B}(\mp \Delta \hat{\psi}), \tag{40}$$

where $\psi_i = \psi(C_i)$, $i = 0, \ldots, n+1$ with $\psi_{n+1} = \psi_S$, $\Delta \hat{\psi} = (\psi_{i+1} - \psi_i)/V_{\text{th}}$ and $\mathcal{B}(z) = z/(e^z - 1)$ is the Bernoulli function. Plugging (40) back into (35), the nodal flux at an internal node reads

$$\Phi_i = q D_\nu \frac{\mathcal{B}(\pm \Delta \hat{\psi}) \nu_{i+1} - \mathcal{B}(\mp \Delta \hat{\psi}) \nu_i}{d_i}, \qquad i = 1, \ldots, n-1, \tag{41}$$

where $\nu_k = \nu(C_k)$, $k = 0, \ldots, n+1$ with $\nu_0 \equiv \nu_D$ and $\nu_{n+1} \equiv \nu_S$. The flux at the Dirichlet contact is given by

$$\Phi_0 = q D_\nu \frac{\mathcal{B}(\pm \Delta \hat{\psi}) \nu_1 - \mathcal{B}(\mp \Delta \hat{\psi}) \nu_D}{d_0}, \tag{42}$$

while equation (39) for the flux at the Schottky contact gives, after some algebra,

$$\Phi_n = q D_\nu \left[\frac{\mathcal{B}(\pm \Delta \hat{\psi}) \nu_S - \mathcal{B}(\mp \Delta \hat{\psi}) \nu_n}{1 + \frac{D_\nu}{\nu_\nu d_n} \mathcal{B}(\pm \Delta \hat{\psi})} \right]. \tag{43}$$

We point out that (43) is the exact discrete counterpart of the formula which describes the physics of a Schottky contact according to the theory of thermoionic emission and diffusion [7]. We notice also that the discrete maximum principle stated in Proposition 1 for the Slotboom variables carries over also to the formulation with the n and p variables. Indeed, the matrix for this latter case is obtained by a postmultiplication of the matrix $\mathbf{M}$ by a *positive* diagonal matrix whose entries are given by $D_{ii} = n_{\text{intr}} e^{\pm \psi_i / V_{\text{th}}}$, which corresponds to a column scaling of $\mathbf{M}$.

5. NUMERICAL RESULTS

We demonstrate the effectiveness of the procedures described in the previous sections on the simulation of a one-dimensional `CdTe` semiconductor slab. We remark that this choice is by no means restrictive for the numerical method, which is indeed valid also in the multidimensional case, but is dictated by the physics of the problem at hand. The device under test is employed in real applications as a monocrystal module for all-optical processing [21], and its simulation represents a very stiff problem, as will be evidenced by numerical results.

The device length L is 0.5 [cm] and the applied voltage is $\Delta V = -2000$ V. The mobilities for electrons and holes are $\mu_n = 1200$ [cm^2/(Vs)] and $\mu_p = 100$ [cm^2/(Vs)], respectively. The energy gap of the material is $E_g = 1.52$ [eV] and its permettivity is $\varepsilon = 10.2 \cdot \varepsilon_0$, ε_0 being the dielectric constant of vacuum. The background doping profile of the device is zero everywhere. Three levels of trapping states are considered, characterized by the data in Table I, where $\Delta\psi_{b_k}$, $k = 1, \ldots, 3$ denotes the distance between the kth trapping level and the corresponding (conduction (a) or valence (b)) band.

We focus our attention on the study of the transient developed by the device as a consequence of an external illumination by a light source placed in the middle of the slab. This source term is modeled by the space–time gaussian $G^{\text{opt}}(x, t) = G_0 e^{-(t-T)^2/(2\sigma_t^2)} e^{-(x-L/2)^2/(2\sigma_x^2)}$, where $G_0 = 10^{21}$ [cm^{-3}s^{-1}] is the peak value, $\sigma_x = 0.025$ [cm] is the spatial variance, $\sigma_t = 1.5 \times 10^{-9}$ [s] is the time variance, and $T = 20 \times 10^{-9}$ [s] is the peak time of the light source.

TABLE 1
Traps Data for `CdTe`

	(a) Donor-type traps	
	Trap #1	Trap #2
C_n^D [cm^3 s^{-1}]	1.9×10^{-7}	1.9×10^{-7}
C_p^D [cm^3 s^{-1}]	8.25×10^{-6}	0
N_D [cm^{-3}]	10^{14}	10^{16}
$\Delta\psi_b$ [eV]	0.76	0.1
	(b) Acceptor-type trap	
	Trap #3	
C_n^A [cm^3 s^{-1}]	0	
C_p^A [cm^3 s^{-1}]	8.25×10^{-6}	
N_A [cm^{-3}]	1.005×10^{16}	
$\Delta\psi_b$ [eV]	0.14	

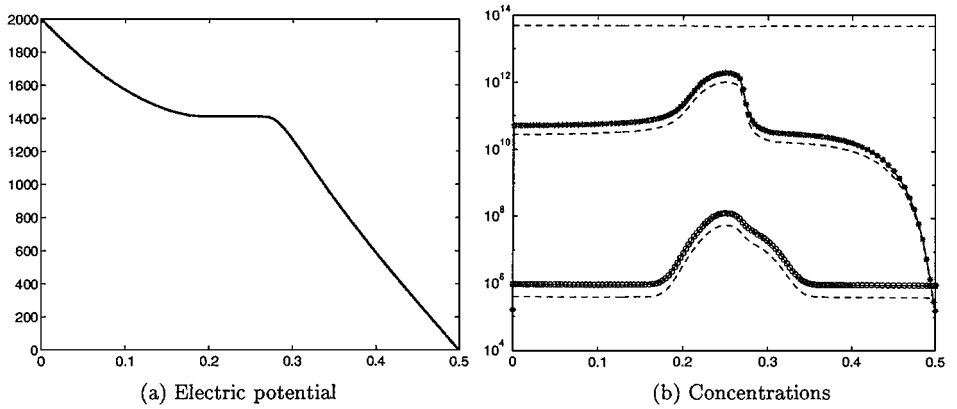

FIG. 1. Potential [V] and concentrations [cm^{-3}]. The dimension of the x-axis is [cm].

In order to catch the very fast transient we set the time step $\Delta t = 5 \times 10^{-10}$ [s] and we ran the computer program for 100 time steps starting from an initial condition corresponding to the given applied voltage but with the light off (dark condition). Moreover, the mesh for the spatial discretization was chosen nonuniform with a maximum mesh size $h_M = 32 \times 10^{-3}$ [cm] in the middle and a minimum mesh size $h_m = 10^{-3}$ [cm] near the boundaries in order to properly describe the expected boundary layers for both carriers and traps. Figures 1a and 1b show the distributions of the electric potential and the concentrations of the free and trapped carriers at the final time level, respectively.

The electrons correspond to the starred line, the holes to the circled line, the trapped carriers to the three dashed lines. In particular observe that the trapping states at mid-gap (top line) are almost completely full while the other two levels, donor level (dashed line, middle) and acceptor level (dashed line, bottom) are actually almost empty. Note also that the spatial distribution of these two latter trapped carriers closely resembles the corresponding ones for the free carrier and the presence of sharp boundary layers. In Fig. 2a we plot the time evolution of the free carriers at about the middle of the semiconductor device, and in Fig. 2b we plot the electric potential at the same position. In the next couple of figures the time

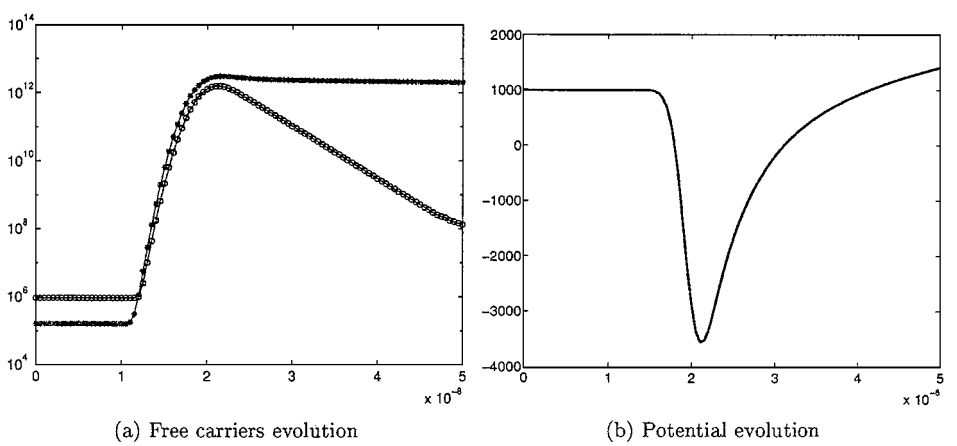

FIG. 2. Free carriers [cm^{-3}] and potential [V]. The dimension of the x-axis is [s].

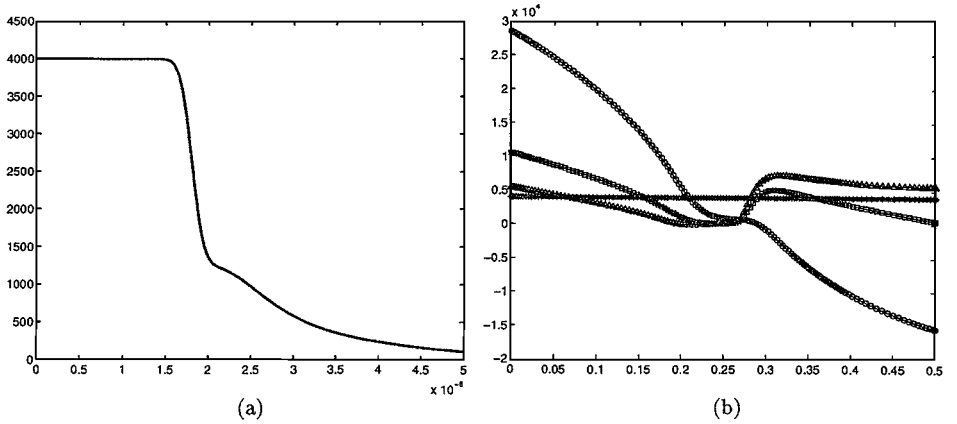

FIG. 3. Electric field [V cm^{-1}]. (a) Time evolution at $x = 0.249$ cm. (b) Space–time distribution. The dimensions of the x-axis are [s] (a) and [cm] (b).

evolution of the electric field at about the middle of the slab and the spatial distribution at the time levels $t_k = k\Delta t$ ($k = 0(*), 50(\circ), 75(\square), 100(\triangle)$) are plotted, respectively. Notice in particular in Fig. 3a the zero-field condition which is exploited in real applications to devise an optically activated electro-optical modulation [21]. The attitude of the device at extending in time the existence of such a zero-field region is also profitably employed to design time-adjustable logical optical gates. As far as the numerics is concerned, Fig. 4a displays the distribution of the eigenvalues of the Schur complement matrix (10), which have been computed run-time using the Matlab **`eig`** intrinsic function. Notice the clustering of the spectrum around the value 1 due to the inversion of elliptic operators. This property reflects into a dramatic improvement of the convergence of GMERS, which actually takes no more than one to two iterations to fulfill the stopping criterion.

Figure 4b shows the convergence history of the external Gauss–Seidel loop for the solution of the steady-state condition with the light on in terms of the maximum potentials variation (electric potential and quasi-Fermi levels) between two successive iterations. We stress that this condition is the stiffest one for the numerical scheme due to the very large values attained by the generation term corresponding to $G^{\mathrm{opt}}(x, T)$. Notice also that the error values must

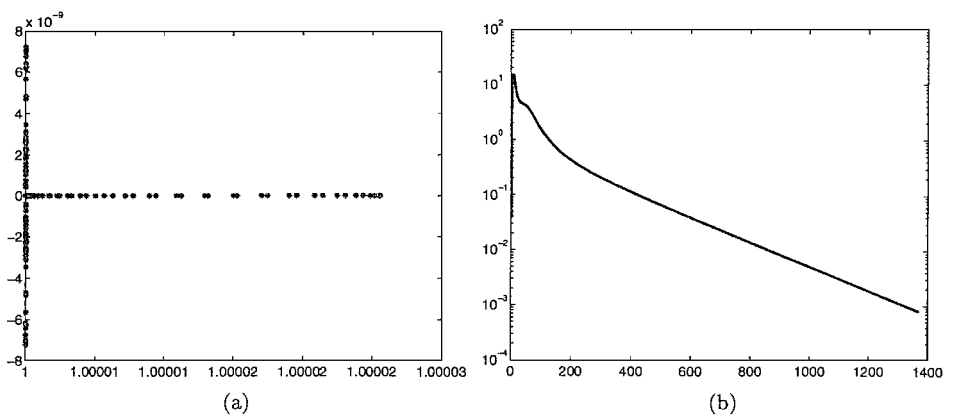

FIG. 4. Eigenvalues and G–S iterations. (a) Eigenvalues. (b) Gauss–Seidel iterations.

be compared with the very large absolute values of the potentials, so that a variation of 10^{-3} is to be regarded as very small and satisfactory for the accuracy of the solution.

ACKNOWLEDGMENTS

The authors gratefully acknowledge Prof. M. Martinelli, director of CORECOM, and Dr. G. Ghislotti for having stimulated this work, and also Dr. S. Pietralunga and the other people of CORECOM for many enlightening discussions about the physical problem and its mathematical modeling. We also do wish to thank the referees for several helpful remarks and comments. This research has been supported by MURST 40% and MURST 60% research funds, by the C.N.R. grants in the Special Project "Metodi Matematici in Fluidodinamica e Dinamica Molecolare," and by CORECOM (Consorzio Ricerche Elaborazione Commutazione Ottica Milano).

REFERENCES

1. U. Ascher, P. A. Markowich, C. Schmeiser, H. Steinrück, and R. Weiss, Conditioning of the steady state semiconductor device problem, *SIAM J. Appl. Math.* **49**, 165 (1989).
2. R. E. Bank and D. J. Rose, Global approximate Newton methods, *Numer. Math.* **37**, 279 (1981).
3. J. Baranger, J. F. Maitre, and F. Oudin, "Application de la théorie des éléments finis mixtes à l'étude d'une classe de schémas aux volumes différences finis pour les problèmes elliptiques. *C. R. Acad. Sci. Paris* **319**, série I, 401 (1994).
4. Deleted in proof.
5. F. Bosisio, E. Gatti, R. Sacco, and F. Saleri, Exponentially fitted mixed finite volumes for energy-balance models in semiconductor device simulation, in *ENUMATH97, Proceedings of the Second European Conference on Numerical Mathematics and Advanced Applications*, edited by H. F. Bock, G. Kanschat, R. Rannacher, F. Bruzzi, R. Glowinski, Y. A. Kuznetsov, and J. Perieaux (World Scientific Publishing Co., XII, Singapore, 1998), p. 188.
6. F. Brezzi and M. Fortin, *Mixed and Hybrid Finite Element Methods* (Springer-Verlag, New York, 1991).
7. C. R. Crowell and S. M. Sze, Current transport in metal-semiconductor barriers, *Solid State Electron.* **9**, 1035 (1966).
8. R. S. Falk and J. E. Osborn, Error estimates for mixed methods, *Rev. Française Automat. Informat. Recherche Opérationnelle Anal. Numér.* **14**, 249 (1980).
9. D. Gilbarg and N. S. Trudinger, *Elliptic Partial Differential Equations of Second Order* (Springer-Verlag, Berlin, 1983).
10. G. Ghislotti, S. Pietralunga, L. Ripamonti, R. Sacco, S. Micheletti, and F. Bosisio, Time-resolved photocurrent and electric field measurements in high resistivity CdTe, *J. Appl. Phys.* **87**, 322 (2000).
11. H. K. Gummel, A self-consistent iterative scheme for one-dimensional steady-state calculations, *IEEE Trans. Electr. Dev*. **ED-11**, 455 (1964).
12. J. J. Jerome, *Analysis of Charge Transport. A Mathematical Study of Semiconductor Devices* (Springer, Berlin, Heidelberg, 1996).
13. T. Kerkhoven, A proof of convergence of Gummel's algorithm for realistic boundary conditions. *SIAM J. Numer. Anal*. **23**, 1121 (1986).
14. T. Kerkhoven, and Y. Saad, On acceleration methods for coupled nonlinear elliptic systems. *Numer. Math*. **60**, 525 (1992).
15. P. A. Markowich, *The Stationary Semiconductor Device Equations* (Springer, Wien, 1986), *j. Appl. Phys. 8th*, 322 (2000).
16. P. A. Markowich, C. A. Ringhofer, and C. Schmeiser, *Semiconductor Equations* (Springer-Verlag, Wien, New York, 1990).
17. S. Micheletti, A. Quarteroni, and R. Sacco, Current-Voltage Characteristics Simulation of Semiconductor Devices using Domain Decomposition, *J. Comp. Phys*. **119**, 46 (1995).

18. S. Micheletti and R. Sacco, New developments in the numerical approximation of the drift-diffusion semiconductor device equations, in *ENUMATH97, Proceedings of the Second European Conference on Numerical Mathematics and Advanced Applications*, edited by H. F. Bock, G. Kanschat, R. Rannacher, F. Bruzzi, R. Glowinski, Y. A. Kuznetsov, and J. Perieaux (World Scientific Publishing Co., XII, Singapore, 1998), p. 469.
19. S. Micheletti and R. Sacco, Stabilized mixed finite elements for fluid models in semiconductors, *Comput. Visualization Sci.* **2**, 139 (1999).
20. S. Micheletti, R. Sacco, and F. Saleri, On some mixed finite element methods with numerical integration, submitted for publication.
21. S. Pietralunga, P. Boffi, M. Martinelli, CdTe: In monocrystal modules for all-optical processing, *J. Nonlinear Opt. Phys. Mater*. **5**(2), 247 (1996).
22. A. Quarteroni and A. Valli, *Numerical Approximation of Partial Differential Equations* (Springer-Verlag, Berlin, 1994).
23. P. A. Raviart and J. M. Thomas, A mixed finite element method for second order elliptic problems, in *Mathematical Aspects of the Finite Element Method*, edited by I. Galligani and E. Magenes, Lect. Notes in Math (Springer-Verlag, New York, 1977), Vol. 606, p. 292.
24. B. I. Reznikov and G. V. Tsarenkov, Inversion of an electric field near the illuminated anode of a metal-semiconductor diode, *Semiconductors* **27**, 699 (1993).
25. Y. Saad and M. H. Schultz, GMRES: A generalized minimal residual method for solving nonsymmetric linear systems, *SIAM J. Sci. Stat. Comput.* **7**, 856 (1986).
26. W. Shockley and W. T. Read, Jr., Statistics of the recombinations of holes and electrons, *Phys. Rev.* **87**(5), 835 (1952).
27. R. Sacco and F. Saleri, Exponentially fitted mixed finite volume methods for convection–diffusion problems, in *Ninth International Conference on Finite Elements in Fluids, New Trends and Applications*, edited by M. Morandi Cecchi, K. Morgan, J. Periaux, B. A. Schrefler, and O. C. Zienkiewicz (1995), p. 1587.
28. R. Sacco and F. Saleri, Mixed finite volume methods for semiconductor device simulation, *Numer. Meth. Part. Diff. Eq.* **13**, 215 (1997).
29. R. Sacco and F. Saleri, Stabilized mixed finite volume methods for convection–diffusion problems, *East–West J. Numer. Math.* **5**(4), 291 (1997).
30. D. L. Scharfetter and H. K. Gummel, Large-signal analysis of a silicon Read diode oscillator, *IEEE Trans. Electr. Dev*. **ED-16**, 64 (1969).
31. S. Selberherr, *Analysis and Simulation of Semiconductor Devices* (Springer-Verlag, Wien, New York, 1984).
32. J. W. Slotboom, Computer-Aided Two Dimensional Analysis of Bipolar Transistors, *IEEE Trans. Electr. Dev*. **ED-20**, 669 (1973).
33. S. M. Sze, *Physics of Semiconductor Devices* (Wiley-Interscience, New York, 1981), 2nd ed.
34. T. Takebe, J. Saraie, and H. Matsunami, Detailed characterization of deep centers in `CdTe`: Photoionization and thermal ionization properties, *J. Appl. Phys*. **53**, 457 (1982).
35. R. S. Varga, *Matrix Iterative Analysis* (Prentice-Hall, Englewood Cliffs, NJ, 1962).